Strength, Fracture and Complexity 7 (2011) 13–31
DOI 10.3233/SFC-2011-0120
IOS Press

Energy emissions from brittle fracture: Neutron measurements and geological evidences of piezonuclear reactions

A. Carpinteri [a,*], G. Lacidogna [a], A. Manuello [a] and O. Borla [a,b]
[a] *Politecnico di Torino, Department of Structural Engineering and Geotechnics, Torino, Italy*
[b] *Istituto Nazionale di Fisica Nucleare, Torino, Italy*

Received 4 October 2010
Accepted 21 February 2011

Abstract. Neutron emission measurements, by means of ^{3}He devices and neutron bubble detectors, were performed during three different kinds of compression tests on brittle rocks: (i) under displacement control, (ii) under cyclic loading and (iii) by ultrasonic vibration. The material used for the tests was Green Luserna Granite. Since the analyzed material contains iron, our conjecture is that piezonuclear fission reactions involving fission of iron into aluminum, or into magnesium and silicon, should have occurred during compression damage and failure. This hypothesis is confirmed by Energy Dispersive X-ray Spectroscopy (EDS) tests conducted on Luserna Granite specimens. It is also interesting to emphasize that the present natural abundances of aluminum (≈8%), and silicon (28%) and scarcity of iron (≈4%) in the continental Earth's crust should be possibly due to the piezonuclear fission reactions considered above.

Keywords: Neutron emission, piezonuclear reactions, rocks crushing failure, energy dispersive X-ray spectroscopy, plate tectonics, element evolution

1. Introduction

We deal with a new topic in the scientific literature: piezonuclear neutron emissions from brittle rock specimens under mechanical loading. The phenomenon is analyzed from an experimental point of view. In the scientific community some studies have been already conducted on the different forms of energy emitted during the failure of brittle materials. They are based on the signals captured by the acoustic emission measurement systems, or on the detection of the electromagnetic charge. On the other hand, only very recently piezonuclear neutron emissions from very brittle rock specimens in compression have been discovered in solids under compression [1–3] and in liquids during cavitation [4,5].

In this paper, after summarizing the preliminary results already presented in [1–3], involving compression tests on prismatic specimens of Carrara Marble and Green Luserna Granite, we present new experiments, using ^{3}He neutron detectors and bubble type BD thermodynamic neutron detectors, performed on brittle rock test specimens. We carried out three different kinds of compression tests: (i) under displacement control, (ii) under cyclic loading and (iii) by ultrasonic solicitations. The material used for

*Address for correspondence: A. Carpinteri, Politecnico di Torino, Department of Structural Engineering and Geotechnics, Corso Duca degli Abruzzi 24, 10129 Torino, Italy. E-mail: alberto.carpinteri@polito.it.

the compression tests was non-radioactive Green Luserna Granite, with different specimen size and shape and consequently with different brittleness numbers. The compression tests were performed at the Fracture Mechanics Laboratory of the Politecnico of Torino, while the ultrasonic test at the Medical and Environmental Physics Laboratory of the University of Torino.

For specimens of larger dimensions, neutron emissions, detected by ^{3}He, were found to be of about one order of magnitude higher than the ordinary natural background level at the time of the catastrophic failure. As regards test specimens with more ductile behaviour, neutron emissions significantly higher than the background level were found. These piezonuclear reactions are affected by the different modalities of energy release during the tests. For specimens with sufficiently large size and slenderness, relatively large energy release is expected, and hence a higher probability of neutron emissions at the time of failure. Furthermore, during compression tests under cyclic loading, an equivalent neutron dose, analysed by neutron bubble detectors, about two times higher than the ordinary background level was found at the end of the test.

Finally, by using an ultrasonic horn suitably joined with the specimen, an ultrasonic test was carried out on a Green Luserna Granite specimen in order to produce continuing vibration at 20 kHz. Three hours after the beginning of the test, an equivalent neutron dose about three times higher than the background level was found.

Moreover, Energy Dispersive X-ray Spectroscopy (EDS) was performed on different samples of external or fracture surfaces belonging to specimens used in the preliminary piezonuclear tests [6]. For each sample, different measurements of the same crystalline phases (phengite or biotite) were performed in order to get averaged information of the chemical composition and to detect possible piezonuclear transmutations from iron to lighter elements. The samples were carefully chosen to investigate and compare the same minerals before and after the crushing failure. Phengite and biotite, that are rather common in the Luserna Granite (20% and 2%, respectively), were considered owing to the high iron concentration in their chemical compositions. The results of EDS analyses show that, on the fracture surface samples, a considerable reduction in the iron content ($\approx$25%) is counterbalanced by a nearly equal increase in Al, Si and Mg concentrations.

Since the analyzed material contains iron, our conjecture is that piezonuclear fission reactions involving fission of iron into aluminum, or into magnesium and silicon, should have occurred during compression on the tested specimens. The present natural abundances of aluminum ($\approx$8%), and silicon (28%) and scarcity of iron ($\approx$4%) in the continental Earth's crust are possibly due to the piezonuclear fission reactions considered above.

These reactions would be activated where the environment conditions (pressure and temperature) are particularly severe, and mechanical phenomena of fracture, crushing, fragmentation, comminution, erosion, friction, etc., may occur. If we consider the evolution of the percentages of the most abundant elements in the Earth crust during the last 4.5 billion years, we realize that iron and nickel have drastically diminished, whereas aluminum, silicon and magnesium have as much increased. It is also interesting to realize that such increases have developed mainly in the tectonic regions, where frictional phenomena between the continental plates occurred [1–3,7].

2. Neutron emission detection technique

Since neutrons are electrically neutral particles, they cannot directly produce ionization in a detector, and therefore cannot be directly detected. This means that neutron detectors must rely upon a conversion process where an incident neutron interacts with a nucleus to produce a secondary charged particle.

These charged particles are then detected, and from them the neutrons presence is deduced. For an accurate neutron evaluation, a ^{3}He proportional counter and a set of passive neutron detectors, based on superheated bubble detection technique, insensitive to electromagnetic noise, were employed.

2.1. ^{3}He proportional counter

The ^{3}He detector used in the tests is a ^{3}He type (Xeram, France) with electronics of preamplification, amplification, and discrimination directly connected to the detector tube. The detector is powered with high voltage power supply (about 1.3 kV) via NIM (Nuclear Instrument Module) module. The logic output producing the TTL (transistor–transistor logic) pulses is connected to a NIM counter. The logic output of the detector is enabled for analog signals exceeding 300 mV. This discrimination threshold is a consequence of the sensitivity of the ^{3}He detector to the gamma rays ensuing neutron emission in ordinary nuclear processes. This value has been determined by measuring the analog signal of the detector by means of a Co-60 gamma source. The detector is also calibrated for the measurement of thermal neutrons; its sensitivity is 65 cps/$n_{thermal}$ ($\pm 10\%$ declared by the factory), i.e., the flux of thermal neutrons was 1 thermal neutron/s cm^2, corresponding to a count rate of 65 cps.

2.2. Neutron bubble detectors

A set of passive neutron detectors insensitive to electromagnetic noise and with zero gamma sensitivity was used. The dosimeters, based on superheated bubble detectors (BTI, ON, Canada) (Bubble Technology Industries (1992)) [8], are calibrated at the factory against an AmBe (Americium–Beryllium) source in terms of NCRP38 [9]. Bubble detectors are the most sensitive, accurate neutron dosimeters available that provide instant visible detection and measurement of neutron dose. Each detector is composed of a polycarbonate vial filled with elastic tissue equivalent polymer, in which droplets of a superheated gas (Freon) are dispersed. When a neutron strikes a droplet, the latter immediately vaporizes, forming a visible gas bubble trapped in the gel. The number of droplets provides a direct measurement of the equivalent neutron dose with an efficiency of about 20%. These detectors are suitable for neutron dose measurements, in the energy range of thermal neutrons ($E = 0.025$ eV, BDT type) and fast neutrons ($E > 100$ keV, BD-PND type).

3. Preliminary tests on prismatic specimens of Carrara Marble and Green Luserna Granite

Preliminary tests on prismatic specimens were presented in previous contributions, recently published [1–3], and related to piezonuclear reactions occurring in solids containing iron – samples of granite rocks – in compression. The materials selected for the compression tests were Carrara Marble (calcite) and Green Luserna Granite (gneiss). This choice was prompted by the consideration that, test specimen dimensions being the same, different brittleness numbers [10] would cause catastrophic failure in granite, not in marble. The test specimens were subjected to uniaxial compression to assess scale effects on brittleness [11].

Four test specimens were used, two made of Carrara Marble and two made of Luserna Granite (Fig. 1). All of them were of the same size and shape, measuring $6 \times 6 \times 10$ cm^3. The same testing machine was used on all the test specimens: a standard servo-hydraulic press with a maximum capacity of 500 kN, equipped with control electronics. This machine makes it possible to carry out tests in either load control or displacement control. The tests were performed in piston travel displacement control by setting, for

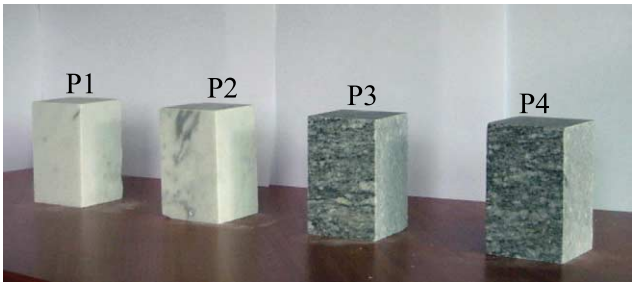

(a)

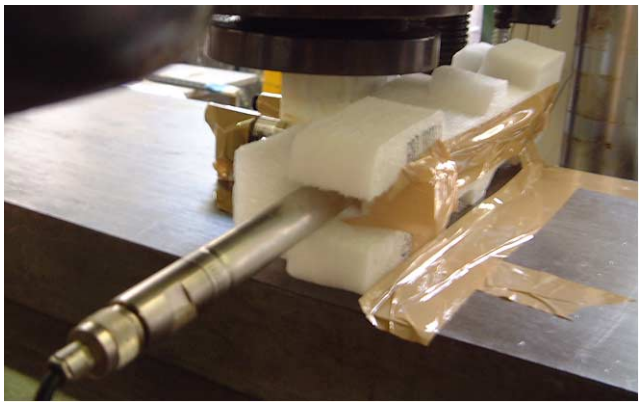

(c)

(b)

Fig. 1. The test specimens analysed, two of Carrara Marble (P1, P2) and two of Luserna Granite (P3, P4), measured $6\times6\times10\,\text{cm}^3$ (a). Baldwin servo-controlled press used for the compression tests (b). ^{3}He neutron detector placed in the proximity of test specimen P1 during the test. The detector is enclosed in a polystyrene case for protection against possible impacts due to test specimen failure (c). (Colors are visible in the online version of the article; http://dx.doi.org/10.3233/SFC-2011-0120.)

all the test specimens, a velocity of 0.001 mm/s during compression. Neutron emission measurements were made by means of a ^{3}He detector placed at a distance of 10 cm from the test specimen and enclosed in a polystyrene case, to prevent the results from being altered by impacts or vibrations.

The measurements of neutron emissions obtained on marble yielded values comparable with the background, even at the time of test specimen failure. The neutron measurements obtained on the two granite test specimens, instead, exceeded the background value by about one order of magnitude when catastrophic failure occurred. The first granite test specimen reached at time $T = 32$ min a peak load of ca. 400 kN, corresponding to an average pressure on the bases of 111.1 MPa. When failure occurred, the count rate was found to be: $(28.3 \pm 5.7) \times 10^{-2}$ cps corresponding to an equivalent flux of thermal neutrons of $(43.6 \pm 8.8) \times 10^{-4}$ $n_{thermal}$ $cm^{-2}s^{-1}$. The second granite test specimen reached at time $T = 29$ min a peak load of ca. 340 kN, corresponding to an average pressure on the bases of 94.4 MPa. When failure occurred, the count rate was found to be $(27.2 \pm 5.5) \times 10^{-2}$ cps corresponding to an equivalent flux of thermal neutrons of $(41.9 \pm 8.5) \times 10^{-4}$ $n_{thermal}$ $cm^{-2}s^{-1}$.

These phenomena could be caused by piezonuclear reactions, that occurred in the granite, but did not in the marble. Moreover, granite contains iron, which appears to be the most favourable element for the production of piezonuclear reactions [1–3]. More particularly, the Carrara Marble used in the piezonuclear tests [1–3] contains only iron impurities (not more than 0.07% of Fe_2O_3 as total Fe), Luserna Granite whereas contains a considerable amount of iron oxides ($\approx$3% of Fe_2O_3 as total Fe). For these

reasons the iron content of the Luserna Granite used in the piezonuclear experiments could contribute to the phenomenon in question. These experimental evidences induced the authors to carry out further tests on cylindrical Green Luserna Granite specimens of different size and shape.

4. Experimental set-up

4.1. Compression tests under displacement control

Neutron emissions were measured on nine Green Luserna Granite cylindrical specimens, of different size and shape (Fig. 2, Table 1), denoted with P1, P2, . . . , P9. The tests were carried out by means of a servo-hydraulic press, with a maximum capacity of 1800 kN, working by a digital type electronic control unit. The management software was TESTXPERTII by Zwick/Roel (Zwick/Roel Group, Ulm, Germany), while the mechanical parts are manufactured by Baldwin (Instron Industrial Products Group, Grove City, PA, USA). The force applied was determined by measuring the pressure in the loading cylinder by means of a transducer. The margin of error in the determination of the force is 1%, which

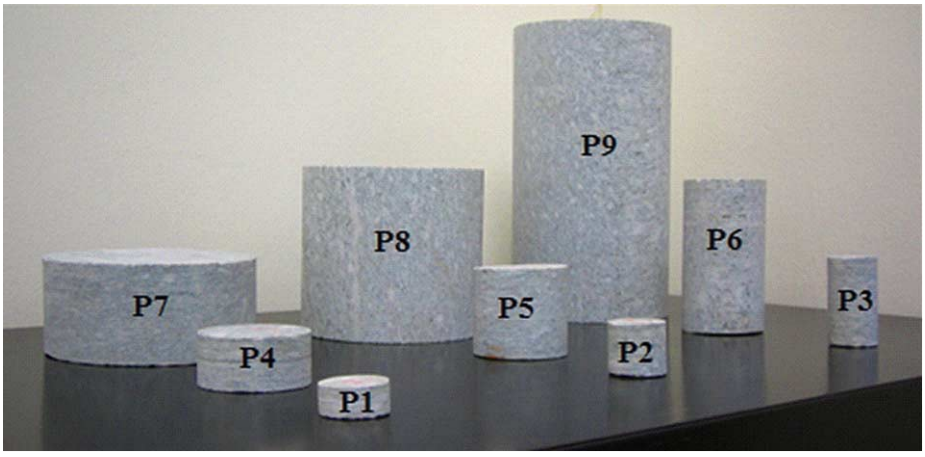

Fig. 2. Green Luserna Granite cylindrical specimens, by varying slenderness and size-scale. (Colors are visible in the online version of the article; http://dx.doi.org/10.3233/SFC-2011-0120.)

Table 1
Characteristics of compression tests under displacement control on Green Luserna Granite specimens

Granite specimen	Geometry of the specimen			Displacement velocity (mm/s)	Peak load (kN)	Time at the peak load (s)
	D (mm)	H (mm)	$\lambda = H/D$			
P1	28	14	0.5	0.001	52.19	735.0
P2	28	28	1	0.001	33.46	1239.0
P3	28	56	2	0.001	41.28	1089.0
P4	53	25	0.5	0.001	129.00	960.0
P5	53	50	1	0.001	139.10	2460.0
P6	53	101	2	0.001	206.50	1180.0
P7	112	60	0.5	0.01	1099.30	231.3
P8	112	112	1	0.01	1077.10	263.5
P9	112	224	2	0.01	897.80	218.6

Table 2
Compression tests under displacement control. Neutron emissions experimental data on Green Luserna Granite specimens

Granite specimen	D (mm)	$\lambda = H/D$	Average neutron background (10^{-2} cps)	Count rate at the neutron emission (10^{-2} cps)
P1	28	0.5	3.17 ± 0.32	8.33 ± 3.73
P2	28	1	3.17 ± 0.32	Background
P3	28	2	3.17 ± 0.32	Background
P4	53	0.5	3.83 ± 0.37	Background
P5	53	1	3.84 ± 0.37	11.67 ± 4.08
P6	53	2	4.74 ± 0.46	25.00 ± 6.01
P7	112	0.5	4.20 ± 0.80	Background
P8	112	1	4.20 ± 0.80	30.00 ± 11.10
P9	112	2	4.20 ± 0.80	30.00 ± 10.00

makes it a class 1 mechanical press. The specimens were arranged with the two smaller surfaces in contact with the press platens, without coupling materials in-between, according to the testing modalities known as "test by means of rigid platens with friction". The tests were performed under displacement control, with the planned displacement velocities ranging from 0.001 to 0.01 mm/s.

The ^{3}He neutron detector was switched on at least one hour before the beginning of each compression test, in order to reach the thermal equilibrium of electronics, and to make sure that the behaviour of the devices was stable with respect to intrinsic thermal effects. The detector was placed in front of the test specimen at a distance of 20 cm and it was enclosed in a polystyrene case of 10 cm thickness in order to avoid "spurious" signals coming from impact and vibration.

A relative measurement of natural neutron background was performed in order to assess the average background affecting data acquisition in experimental room condition. The ^{3}He device was positioned in the same condition of the experimental set up and the background measures were performed fixing at 60 s the acquisition time, during a preliminary period of more than three hours, for a total number of 200 counts. The average measured background level is ranging from $(3.17 \pm 0.32) \times 10^{-2}$ to $(4.74 \pm 0.46) \times 10^{-2}$ cps (see Table 2).

4.2. Compression test under cyclic loading

A Green Luserna Granite specimen ($D = 53$ mm, $H = 53$ mm, $\lambda = 1$) was used. The cyclic loading was programmed at a frequency of 2 Hz and with a load excursion from a minimum load of 10 kN to a maximum of 60 kN. With respect to the tests performed under displacement control, neutron emissions from compression test under cyclic loading were performed by using neutron bubble detectors. Due to their isotropic angular response, three BDT and three BD-PND detectors were positioned at a distance of about 5 cm, all around the specimen. The detectors were previously activated, unscrewing the protection cap, in order to reach the suitable thermal equilibrium, and they were kept active for all the test duration. Furthermore, a BDT and a BD-PND detector were used as background control during the test.

4.3. Ultrasonic test

A Green Luserna Granite specimen ($D = 53$ mm, $H = 100$ mm, $\lambda = 2$) was connected to the ultrasonic horn by a glued screw inserted in a 5 mm deep hole (Fig. 3). This kind of connection was made in order to achieve a resonance condition, considering the speed of sound in Luserna stone, and the length of the specimen. Ultrasonic irradiation of the specimen was carried out for 3 h. After the

Fig. 3. The Green Luserna Granite specimen connected to the ultrasonic horn. The ultrasonic apparatus (Bandelin HD 2200) consists of a generator that converts electrical energy to 20 kHz ultrasound, and of a transducer that switches this energy into mechanical longitudinal vibration of the same frequency. (Colors are visible in the online version of the article; http://dx.doi.org/10.3233/SFC-2011-0120.)

switching on of the transducer, 10% of the maximum power was reached in 20 min. Successively, the transducer power increased to 20% after one hour, and next reached a maximum level of about 30% after 2 h. Then, the transducer worked in the same power condition up to the end of the test.

5. Experimental results

5.1. Compression tests under displacement control

Neutron measurements of specimen P2, P3, P4, P7 yielded values comparable with the ordinary natural background, while in specimens P1 and P5 the experimental data exceeded the background value by about four times. On the other hand, for specimen P6, P8 and P9, the neutron emissions achieved values one order of magnitude higher than the ordinary background. In Fig. 4, for specimens P6, P8 and P9, the load vs. time diagram, and the neutron count rate evolution are shown. In Table 2, experimental data concerning compression tests on the nine Green Luserna Granite specimens are synthesized. It is a matter of fact that the detected neutron flux, and consequently neutron dose, are inversely proportional to the square of the distance from the source. For these reasons, the ^{3}He device could have underestimated neutron flux intensity. A possible solution to avoid underestimated data acquisition is an experimental measurement by using more than one ^{3}He detector and more bubble dosimeters placed around the test specimens.

5.2. Compression test under cyclic loading

Droplets counting was performed every 12 h and the equivalent neutron dose was calculated. In the same way, the natural background was estimated by means of the two bubble dosimeters used for assessment. The ordinary background was found to be 13.98 ± 2.76 nSv/h.

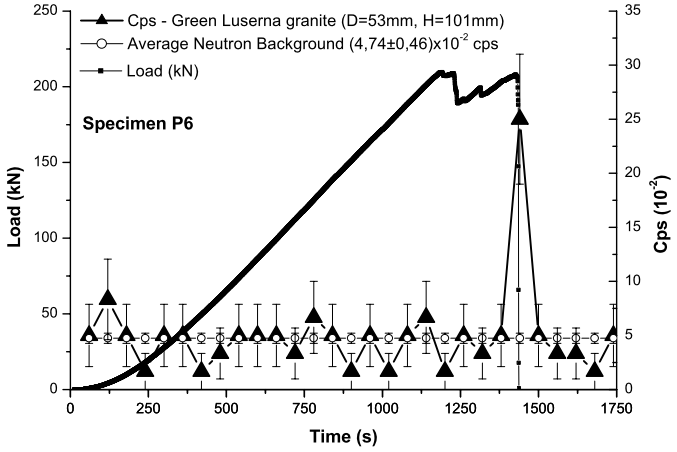

(a)

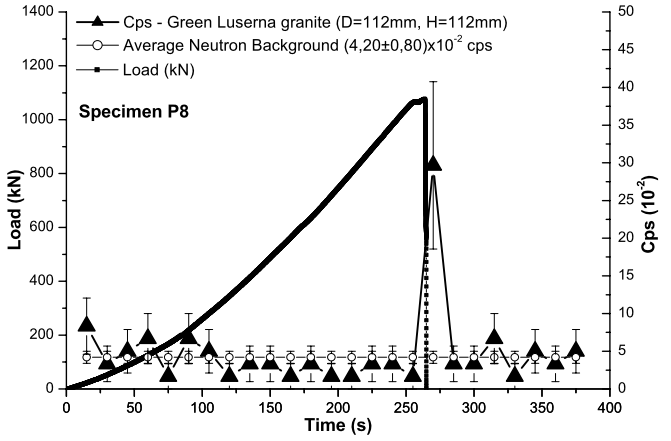

(b)

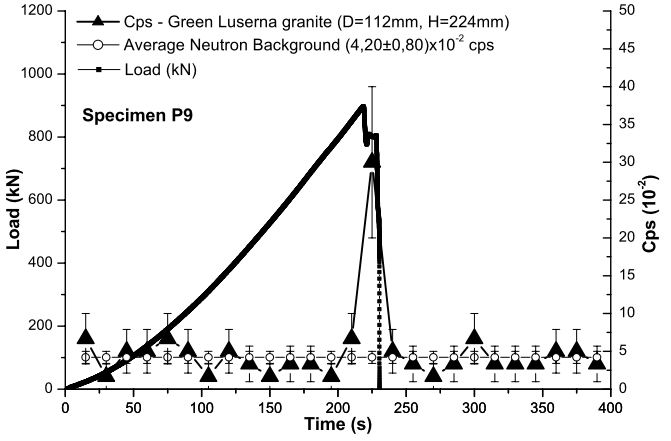

(c)

Fig. 4. Specimens (a) P6, (b) P8 and (c) P9. Load vs. time diagrams, and neutron emissions count rate.

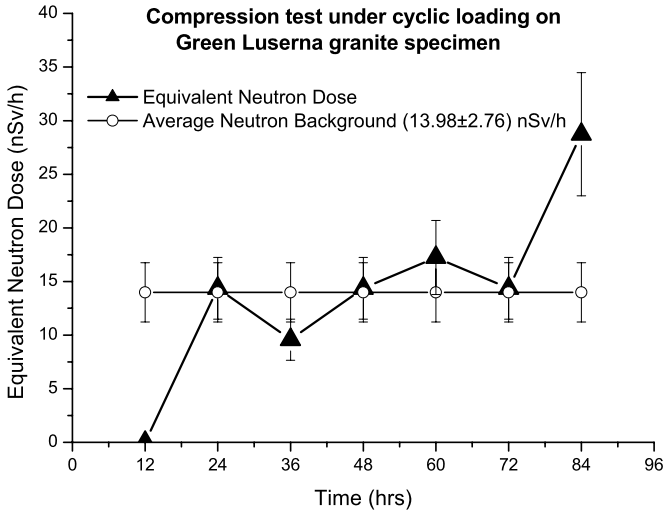

Fig. 5. Compression test under cyclic loading. Equivalent neutron dose variation on Green Luserna Granite specimen.

In Fig. 5 neutron equivalent dose variation, evaluated during the cyclic compression test, is reported. An increment of more than twice with respect to the background level was detected at specimen failure. No significant variations in neutron emissions were observed before the failure. The equivalent neutron dose, at the end of the test, was 28.74 ± 5.75 nSv/h.

5.3. Ultrasonic test

Ultrasonic oscillation was generated by an high intensity ultrasonic horn (Bandelin HD 2200) working at 20 kHz. The device guarantees a constant amplitude (ranging from 10% to 100%) independently of changing conditions within the sample. The apparatus consists of a generator that converts electrical energy to 20 kHz ultrasounds, and of a transducer that switches this energy into mechanical longitudinal vibration at the same frequency.

The ultrasonic test on Green Luserna Granite specimen ($D = 53$ mm, $H = 100$ mm, $\lambda = 2$) was carried out at the Medical and Environmental Physics Laboratory of Experimental Physics Department of the University of Torino. A relative natural background measurement was performed by means of the ^{3}He detector for more than 6 h. The average natural background was of $(6.50 \pm 0.85) \times 10^{-3}$ cps, for a corresponding thermal neutron flux of $(1.00 \pm 0.13) \times 10^{-4}$ $n_{thermal}$ $cm^{-2}s^{-1}$. This natural background level, lower than the one calculated during the compression tests at the Fracture Mechanics Laboratory of the Politecnico of Torino, is in agreement with the location of the experimental Physics Laboratory, which is three floors below the ground level.

During the ultrasonic test, the specimen temperature was monitored by using a multimeter/thermometer (Tektronix mod. S3910). The temperature reached 50°C after 20 min, and then increased up to a maximum level of 100°C at the end of the ultrasonic test. In Fig. 6, the neutron emissions detected are compared with the transducer power trend and the specimen temperature. A significant increment in neutron activity after 130 min from the beginning of the test was measured. At this time, the transducer power reached 30% of the maximum, with a specimen temperature of about 90°C. Some neutron variations were detected during the first hour of the test, but they may be due to ordinary fluctuations of

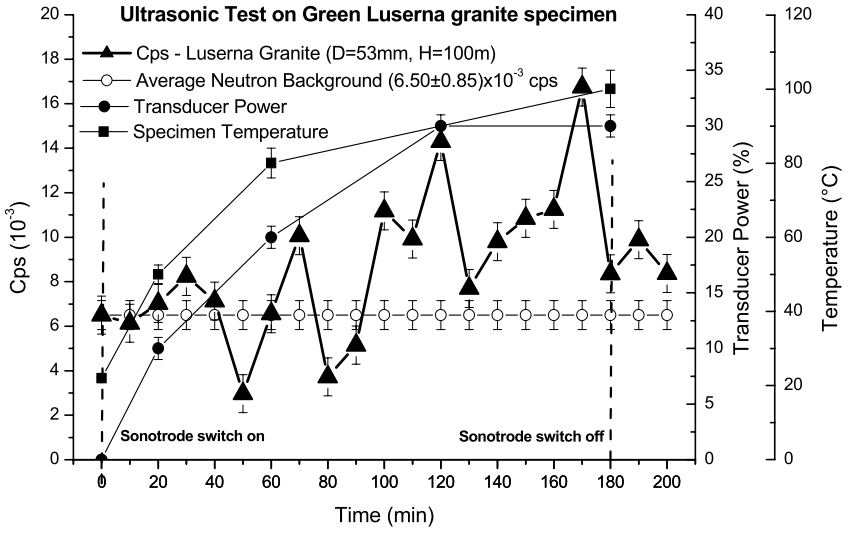

Fig. 6. Ultrasonic test. Neutron emissions compared with the specimen temperature, and with the transducer power trend.

natural background. At the switching off of the sonotrode, the neutron activity decreased to the typical background value.

6. Compositional and microchemical evidence of piezonuclear fission reactions in the rock specimens

Energy Dispersive X-ray Spectroscopy (EDS) was performed on different samples of external or fracture surfaces, belonging to the same specimens of Green Luserna Granite used in the preliminary piezonuclear tests by Carpinteri et al. [1–3]. The tests were conducted in order to correlate the neutron emission from the Luserna Granite with the variations in rock composition due to brittle failure of the granitic gneiss specimens. These analyses lead to get averaged information of the mineral chemical composition and to detect possible piezonuclear transmutations from iron to lighter elements. The quantitative elemental analyses were performed by a ZEISS Supra 40 Field Emission Scanning Electron Microscope (FESEM) equipped with an Oxford X-rays microanalysis. The samples were carefully chosen to investigate and compare the same crystalline phases both before and after the crushing failure. In particular, two crystalline phases, phengite and biotite, were considered due to their high iron content and relative abundances in the Luserna Granite (20% and 2%, respectively) [12].

Luserna “stone” is a leucogranitic orthogneiss, probably from the Lower Permian Age, that outcrops in the Luserna-Infernotto basin (Cottian Alps, Piedmont) at the border between the Turin and Cuneo provinces (North-western Italy) [13]. Characterized by a micro “Augen” texture, it is grey-greenish or locally pale blue in colour. Geologically, Luserna stone pertains to the Dora–Maira massif [13,14], that represents a part of the ancient European margin annexed to the Cottian Alps during Alpine orogenesis. From a petrographic point of view, it is the metamorphic result of a late-Ercinian leucogranitic rock transformation [12,14]. The Luserna stone has a sub-horizontal attitude, with a marked fine-grained foliation that is mostly associated with visible lineation. The mineralogical composition includes K-feldspar (10–25 wt%), quartz (30–40 wt%), albite (15–25 wt%) and phengite (10–20 wt%); subordinated biotite, chlorite, zoisite and/or clinozoisite/epidote (less then 5%). In addition to common accessory phases

(ores, titanite, apatite and zircon), tourmaline, carbonates, rare axinite and frequent fluorite are present [12,15].

In consequence of Luserna stone being a very heterogeneous rock, and in order to assess mass percentage variations in chemical elements such as Fe, Al, Si and Mg, the EDS analyses have been focused on two crystalline phases: phengite and biotite (Fig. 7a and b).

In Fig. 8a, two thin sections obtained from the external surfaces of a portion of one of the tested specimens are shown. The thin sections, finished with a standard petrographic polishing procedure,

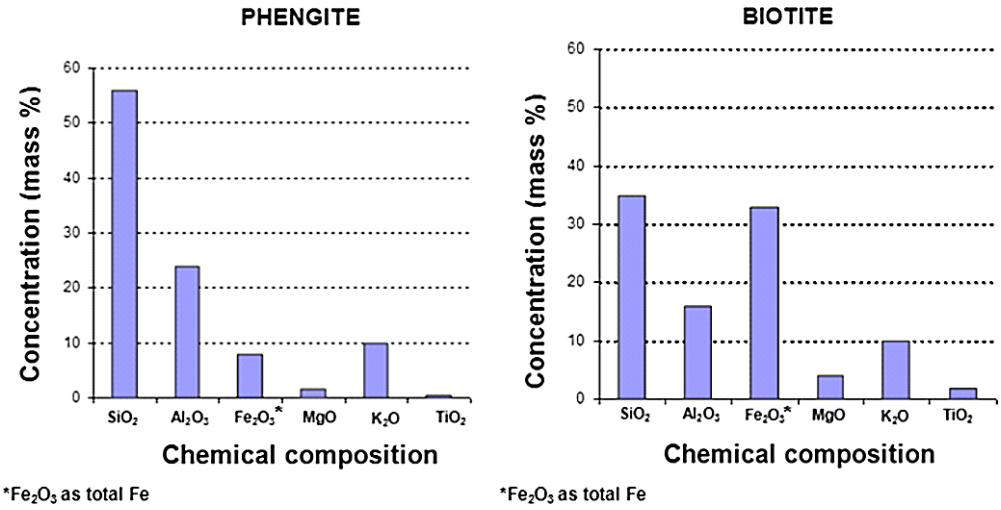

(a) (b)

Fig. 7. (a) The chemical composition of phengite includes: SiO_2 (≈56%), Al_2O_3 (≈24%), Fe_2O_3 and FeO (≈8%) MgO (≈1.5%), Na_2O (≈0.2%) and K_2O (≈10%). (b) The chemical composition of biotite includes: SiO_2 (≈35%), Al_2O_3 (≈16%), Fe_2O_3 and FeO (≈33%), MgO (≈3.5%), TiO_2 (≈1.5%) and K_2O (≈10%). (Colors are visible in the online version of the article; http://dx.doi.org/10.3233/SFC-2011-0120.)

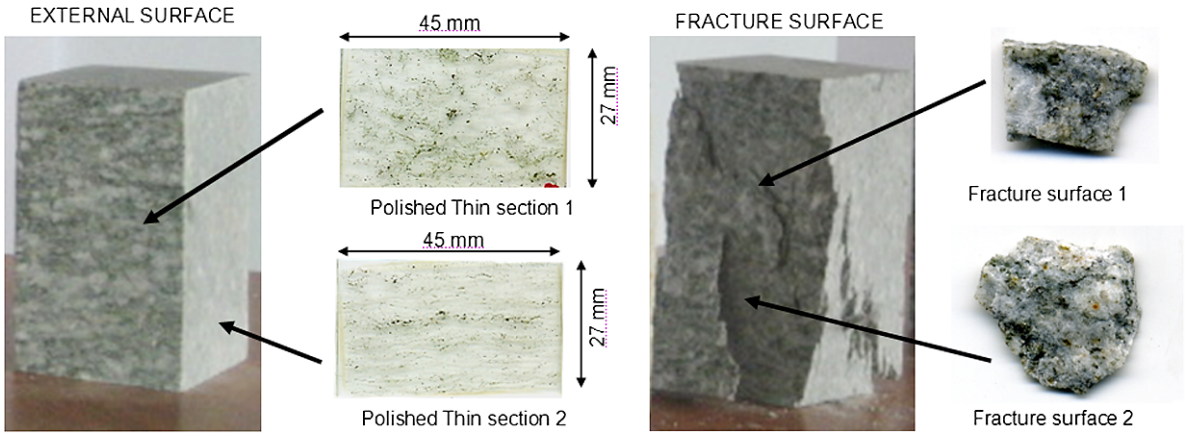

(a) (b)

Fig. 8. (a) Polished thin sections obtained by the external surface of an integer and not fractured portion of the tested specimens [1,3]. (b) Fracture surface belonging to the tested specimens [1–3]. (Colors are visible in the online version of the article; http://dx.doi.org/10.3233/SFC-2011-0120.)

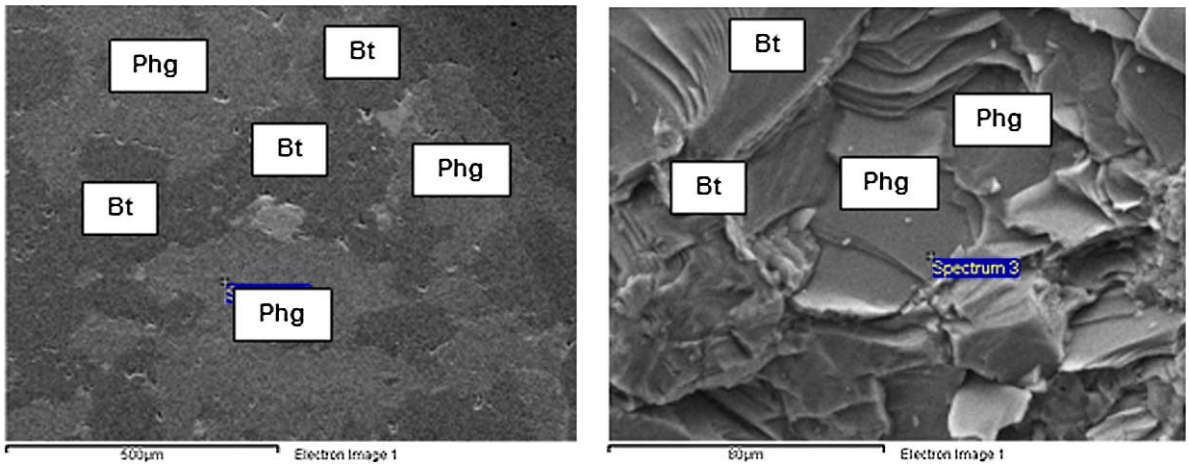

(a) (b)

Fig. 9. FESEM images of phengite and biotite in the case of (a) external and (b) fracture sample. (Colors are visible in the online version of the article; http://dx.doi.org/10.3233/SFC-2011-0120.)

present a rectangular geometry (45 × 27 mm) and are 30 μm thick. In Fig. 8b, two portions of fracture surfaces taken from the tested specimen are shown. For the EDS analyses, several phengite and biotite sites were localized on the surface of the thin sections and on the fracture surfaces. Sixty measurements of phengite crystalline phase, and thirty of biotite were selected and analysed. In Fig. 9a and b, two electron microscope images of phengite and biotite sites, the first in the external sample (thin section 1) and the second on the fracture surface (fracture surface 2), are shown.

6.1. EDS results for phengite

In Fig. 10a and b, the results for the Fe concentrations obtained from the measurements on phengite crystalline phase are shown. Thirty of these measurements were carried out on the polished thin sections as representatives of the external surface samples, whereas the other thirty measurements were carried out on fracture surfaces. It can be observed that the distribution of Fe concentrations for the external surfaces, represented in the graph by squares, show an average value of the distribution (calculated as the arithmetic mean value) equal to 6.20%. In the same graph the distribution of Fe concentrations on the fracture samples (indicated by triangles) shows significant variations. It can be seen that the mean value of the distribution of measurements performed on fracture surfaces is equal to 4.0% and it is considerably lower than the mean value of external surface measurements (6.20%). It is also interesting to note that the two Fe value distributions are separated by at least two standard deviations ($\sigma = 0.37$ in the case of external surfaces and $\sigma = 0.52$ in the case of fracture surfaces).

The iron decrease, considering the mean values of the distributions of phengite composition, is about 2.20%. This iron content reduction corresponds to a relative decrease of 35% with respect to the previous Fe content in phengite (6.20%). Similarly to Fig. 10a, in Fig. 10b the Al mass percentage concentrations are considered in both the cases of external and fracture surfaces. For Al contents, the observed variations show a mass percentage increase approximately equal to that of Fe (compare Fig. 10a and b). The average increase in the distribution, corresponding to the fracture surfaces (indicated by triangles), is about 2.00% of the phengite composition. The average value of Al concentrations changes from 12.50%

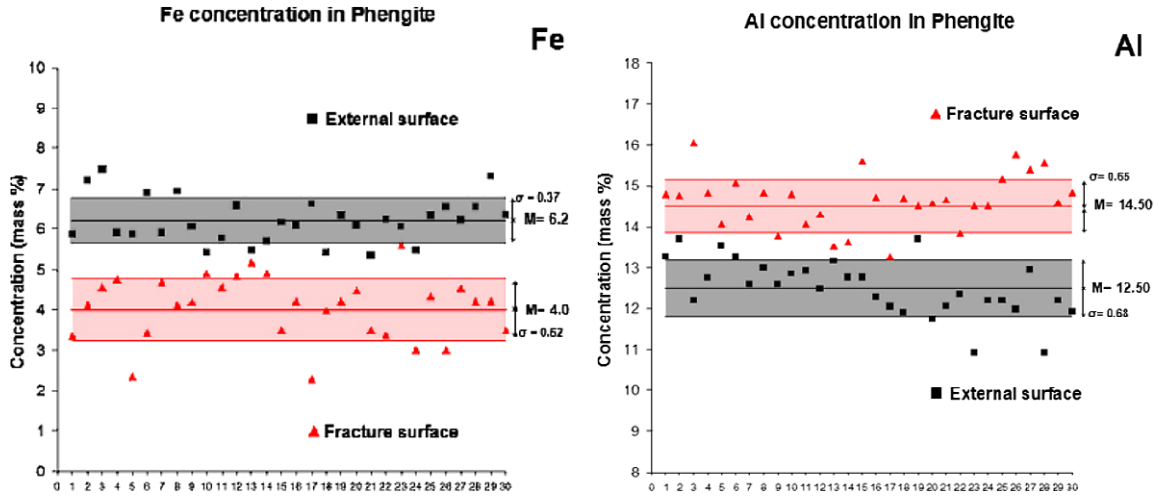

Fig. 10. Fe and Al concentrations in phengite: (a) Fe concentrations on external surfaces (squares) and on fracture surfaces (triangles). The Fe decrease considering the two mean values of the distributions is equal to 2.20%. (b) Al concentrations on external surfaces (squares) and on fracture surfaces (triangles). The Al increase, considering the two mean values of the distributions, is equal to 2.0%. (Colors are visible in the online version of the article; http://dx.doi.org/10.3233/SFC-2011-0120.)

on the external surface to 14.50% on the fracture surface. The relative increase in Al content is equal to 16%.

The evidence emerging from the EDS analyses, that the two values for the iron decrease (−2.20%) and for the Al increase (+2.0%) are approximately equal, is really impressive. This fact is even more evident considering the trends of the other chemical elements constituting the mineral chemistry (excluding H and O) in phengite, because no appreciable variations can be recognized between the average values [6].

6.2. EDS results for biotite

In the Fig. 11a–d the results for Fe, Al, Si and Mg concentrations measured on 30 acquisition points of biotite crystalline phase are shown. These measurements were selected on the polished thin sections as representatives of the uncracked material samples (15 measurements) and of fracture surfaces (15 measurements). It can be observed that the distribution of Fe concentrations for the external surfaces, represented in Fig. 11a by squares, shows an average value of the distribution (calculated as the arithmetic mean value) equal to 21.20%. On the other hand, considering in the same graph the distribution of Fe concentrations on fracture samples (indicated by triangles), it can be seen that the mean value drops to 18.20%. In this case, the iron decrease, considering the mean values of the distributions of biotite composition, is about 3.00%. This iron content reduction (−3.00%) corresponds to a relative decrease of 14% with respect to the previous Fe content (21.20% in biotite). Similarly to Fig. 11a, in Fig. 11b the Al mass percentage concentrations are considered in both cases of external and fracture samples. For Al contents the observed variations show an average increase of about 1.50% in the biotite composition. The average value of Al concentrations changes from 8.10% on the external surface to 9.60% on the fracture surface, with a relative increase in Al content equal to 18%. In Fig. 11c and d it is shown that, in the case of biotite, also Si and Mg contents present considerable variations. Figure 11c shows that the mass percentage concentration of Si changes from a mean value of 18.4% (external surface) to a

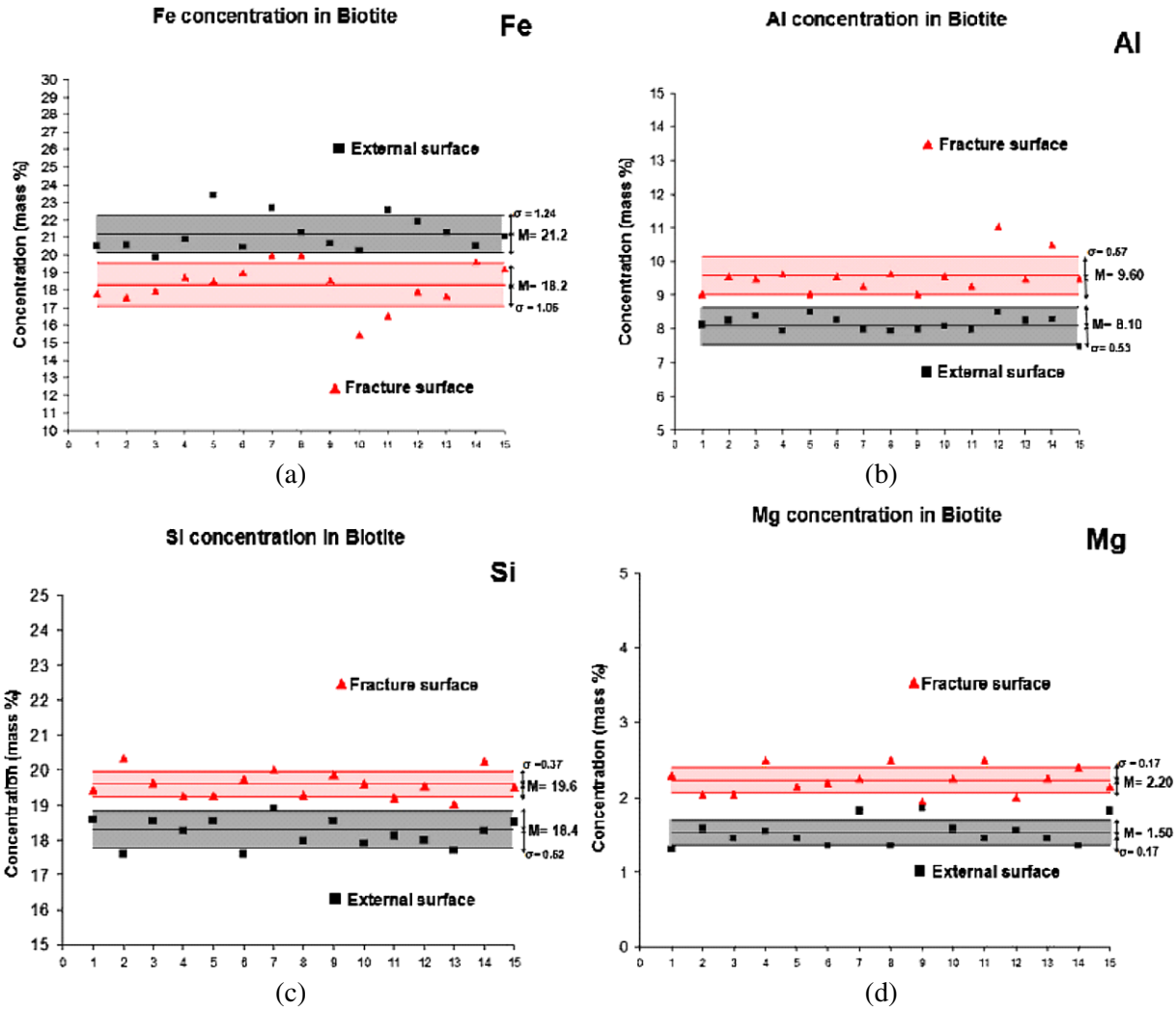

Fig. 11. Fe (a), Al (b), Si (c) and Mg (d) concentrations in biotite are reported for external and fracture surfaces. The iron decrease (−3.00%) in biotite is counterbalanced by an increase in aluminum (+1.50%), silicon (+1.20%) and magnesium (+0.70%). In the case of the other elements no appreciable variations can be recognized between the external and the fracture samples [6]. (Colors are visible in the online version of the article; http://dx.doi.org/10.3233/SFC-2011-0120.)

mean value of 19.60% (fracture surface) with an increase of 1.20%. Similarly, in Fig. 11d the Mg concentration distributions show that the mean value of Mg content changes from 1.50% (external surface) to 2.20% (fracture surface). Therefore, the iron decrease (−3.00%) in biotite is counterbalanced by an increase in aluminum (+1.50%), silicon (+1.20%) and magnesium (+0.70%) [6].

7. Piezonuclear reactions: from the laboratory to the Earth scale

From the results shown in the previous sections and the experimental evidence reported in recent papers [1–3,6], it can be clearly seen that piezonuclear reactions are possible in inert non-radioactive solids.

From the EDS results on fracture samples, the evidences of Fe and Al variations on phengite (Fig. 10) lead to the conclusion that the piezonuclear reaction:

$$\mathrm{Fe}_{26}^{56} \rightarrow 2\mathrm{Al}_{13}^{27} + 2\,\text{neutrons}, \tag{1}$$

should have occurred [1–3,6]. Moreover, considering the evidences for the biotite content variations in Fe, Al, Si, and Mg (Fig. 11), it is possible to conjecture that another piezonuclear reaction, in addition to (1), should have occurred during the piezonuclear tests [1–3,6]:

$$\mathrm{Fe}_{26}^{56} \rightarrow \mathrm{Mg}_{12}^{24} + \mathrm{Si}_{14}^{28} + 4\,\text{neutrons}. \tag{2}$$

Taking into account that granite is a common and widely occurring type of intrusive, Sialic, igneous rock, and that it is characterized by an extensive concentration in the rocks that make up the Earth's crust (≈60% of the Earth's crust), the piezonuclear fission reactions expressed above can be generalized from the laboratory to the Earth's crust scale, where mechanical phenomena of brittle fracture, due to fault collision and subduction, take place continuously in the most seismic areas. This hypothesis seems to find surprising evidence and confirmation from both the geomechanical and the geochemical points of view. The neutron emissions involved in piezonuclear reactions can be detected not only in laboratory experiments, as shown in [1–3], but also at the Earth's crust scale. Recent neutron emission detections have led to consider also the Earth's crust, in addition to cosmic rays, as a relevant source of neutron flux variations [16,17]. Neutron emissions measured at seismic areas in the Pamir region (4200 m asl) exceeded the usual neutron background up to two order of magnitude in correspondence to seismic activity and rather appreciable earthquakes, greater than or equal to the 4th degree in the Richter scale magnitude [18]. This relationship between the processes in the Earth's crust and neutron flux variations has allowed increasing tectonic activity to be detected and methods for short-term prediction and monitoring of earthquakes to be developed [16,17]. Neutron flux variations, in correspondence to seismic activity, may be evidence of changes in the chemical composition of the crust, as a result of piezonuclear reactions. The present natural abundances of aluminum (≈8%), and silicon (28%) and scarcity of iron (≈4%) in the continental Earth's crust are possibly due to the piezonuclear fission reactions considered above.

8. Heterogeneity in the composition of the Earth's crust: Fe and Al reservoir locations

The location of Al and Fe mineral reservoirs seems to be closely connected to the geological periods when different continental zones were formed [19–25]. This fact would seem to suggest that our planet has undergone a continuous evolution from the most ancient geological regions, which currently reflect the continental cores that are rich in Fe reservoirs, to more recent or contemporary areas of the Earth's crust where the concentrations of Si and Al oxides present very high mass percentages [19,26–29]. The main iron reservoir locations (Magnetite and Hematite mines) are reported in Fig. 12a. The main concentrations of Al-oxides and rocky andesitic formations (the Rocky Mountains and the Andes, with a strong concentration of Al_2O_3 minerals) are shown in Fig. 12b together with the most important subduction lines, plate tectonic trenches and rifts [19,23,28]. The geographical locations of main bauxite mines show that the largest concentrations of Al reservoirs can be found in correspondence to the most seismic areas of the Earth (Fig. 12b). The main iron mines are instead exclusively located in the oldest and interior parts of continents (formed through the eruptive activity of the proto-Earth), in geographic

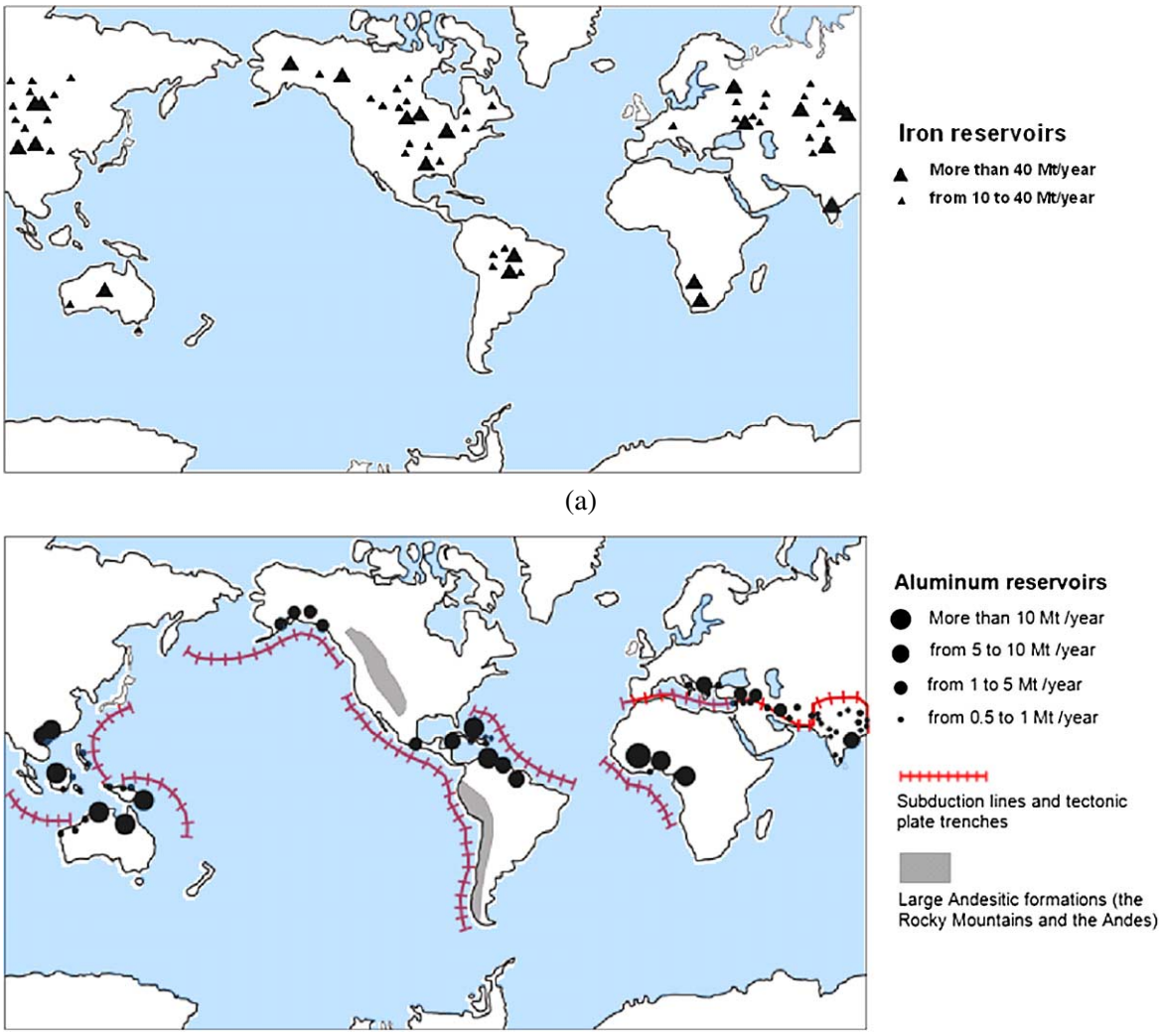

Fig. 12. (a) Locations of the largest iron mines in the world [26,27,29]. Iron ore reservoirs (magnetite and hematite mines) are located in geographic areas with reduced seismic risks and always far from fault lines. (b) The largest aluminum (bauxite) reservoirs are reported together with the main Andesitic formations and most important subduction lines and plate tectonic trenches [19,28]. (Colors are visible in the online version of the article; http://dx.doi.org/10.3233/SFC-2011-0120.)

areas with a reduced seismic risk and always far from the main fault lines. From this point of view, the close correlation between bauxite and andesitic reservoirs and the subduction and most seismic areas of the Earth's crust provides very impressive evidence of piezonuclear effects at the planetary scale.

9. Geochemical evidence of piezonuclear reactions in the evolution of the Earth's crust

Evidence of piezonuclear reactions can be also recognized considering the Earth's composition and its way of evolving throughout the geologic eras. In this way, plate tectonics and the connected plate

collision and subduction phenomena are useful to understand not only the morphology of our planet, but also its compositional evolution [7].

From 4.0 to 2.0 Gyrs ago, Fe could be considered one of the most common bio-essential elements required for the metabolic action of all living organisms. Today, the deficiency of this nutrient suggests it as a limiting factor for the development of marine phytoplankton and life on Earth [22].

Elements such as Fe and Ni in the Earth's protocrust had higher concentrations during the Hadean (4.5–3.8 Gyr ago) and Archean (3.8–2.5 Gyr ago) periods compared to the present values. The Si and Al concentrations instead were lower than those of today [19–21]. In Fig. 13, the evolution in mass percentage concentration of Si, Al, Fe and Ni in the Earth protocrust and crust over the last 4.5 billion years is reported.

Considering the data reported in Fig. 13, it is possible to conjecture, in addition to reactions (1) and (2), another piezonuclear fission reaction that could have taken place in correspondence to plate collision and subduction [7]:

$$\mathrm{Ni}_{28}^{59} \rightarrow 2\mathrm{Si}_{14}^{28} + 3\,\text{neutrons}. \tag{3}$$

Taking into account these considerations, a clear transition from a more basaltic condition (high concentrations of Fe and Ni) to a Sialic one (high concentrations of Al and Si) can be observed during the life time of our planet [7]. The most abrupt changes in element concentrations shown in Fig. 13 appear to be intimately connected to the tectonic activity of the Earth. In particular, the abrupt transitions of 2.5 Gyrs ago coincide with the period of the Earth's largest tectonic activity [7,21].

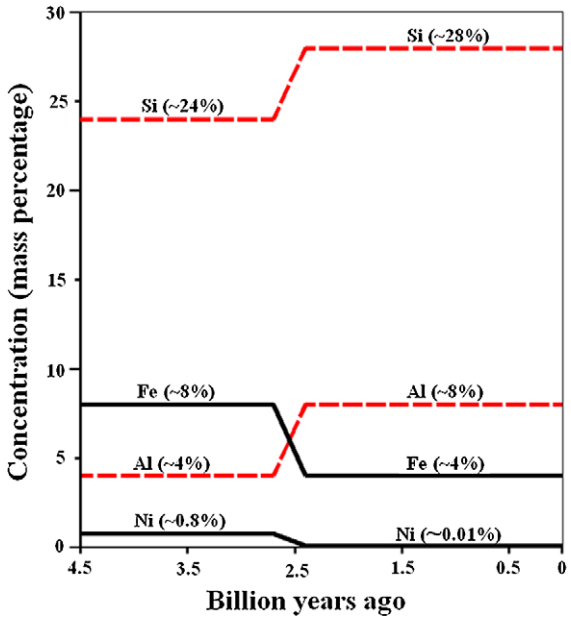

Fig. 13. The estimated mass percentage concentrations of Si, Al, Fe and Ni in the Earth crust during the last 4.5 billion years (age of the planet Earth) [7,19–21,24,30–36]. (Colors are visible in the online version of the article; http://dx.doi.org/10.3233/SFC-2011-0120.)

10. Conclusions

Neutron emission measurements were performed on Green Luserna Granite specimens during mechanical tests. From these experiments, it can be clearly seen that piezonuclear reactions giving rise to neutron emissions are possible in inert non-radioactive solids under loading. In particular, during compression tests of specimens with sufficiently large size, the neutron flux was found to be of about one order of magnitude higher than the background level at the time of catastrophic failure. For test specimens with more ductile behaviour, neutron emissions significantly higher than the background were found. Neutron detection is also confirmed in compression tests under cyclic loading and during ultrasonic vibration.

Our conjecture, also confirmed by the Energy Dispersive X-ray Spectroscopy (EDS) tests, is that piezonuclear fission reactions involving fission of iron into aluminum, or into magnesium and silicon, should have occurred during compression on the tested specimens.

This hypothesis seems to find surprising evidence and confirmation at the Earth crust scale from both geomechanical and geochemical points of view. In this way, the piezonuclear reactions have been considered in order to interpret the most significant geophysical and geological transformations, today still unexplained.

Finally, through experimental and theoretical studies of neutron emission and piezonuclear fission reactions from brittle fracture, it will also be possible to explore new and fascinating application fields, such as short-term prediction and monitoring of earthquakes, production of neutrons for medical use in cancer therapy, disposal of radioactive waste, and even the hypothetical production of clean nuclear energy.

Acknowledgements

The financial support provided by the Regione Piemonte (Italy) RE-FRESCOS Project, is gratefully acknowledged. Special thanks are due to R. Sandrone and A. Chiodoni of the Politecnico di Torino for their kind collaboration in the EDS analysis. The authors wish to thank also D. Madonna Ripa and A. Troia from the National Research Institute of Metrology – INRIM, for their indispensable assistance during the ultrasonic tests.

References

[1] A. Carpinteri, F. Cardone and G. Lacidogna, Piezonuclear neutrons from brittle fracture: early results of mechanical compression tests, *Strain* **45** (2009), 332. Presented at the Turin Academy of Sciences on December 10, 2008, *Proc. Turin Acad. Sci. Ser. V* **33** (2010), 27.

[2] F. Cardone, A. Carpinteri and G. Lacidogna, Piezonuclear neutrons from fracturing of inert solids, *Physics Letters A* **373** (2009), 4158–4163.

[3] A. Carpinteri, F. Cardone and G. Lacidogna, Energy emissions from failure phenomena: mechanical, electromagnetic, nuclear, *Experimental Mechanics* **50** (2010), 1235–1243.

[4] F. Cardone, G. Cherubini and A. Petrucci, Piezonuclear neutrons, *Physics Letters A* **373** (2009), 862–866, see also: F. Cardone et al., http://www.arxiv.org/abs/0710.5115.

[5] F. Cardone and R. Mignani, *Deformed Spacetime*, Springer, Dordrecht, 2007, Chapters 16 and 17.

[6] A. Carpinteri, A. Chiodoni, A. Manuello and R. Sandrone, Compositional and microchemical evidence of piezonuclear fission reactions in rock specimens subjected to compression tests, *Strain*, to appear, doi: 10.1111/j.1475-1305.2010.00767.x.

[7] A. Carpinteri and A. Manuello, Geomechanical and geochemical evidence of piezonuclear fission reactions in the Earth's crust, *Strain*, to appear, doi: 10.1111/j.1475-1305.2010.00766.x.
[8] Bubble Technology Industries, Instruction manual for the Bubble detector, Chalk River, ON, Canada, 1992.
[9] National Council on Radiation Protection and Measurements, Protection against neutron radiation, NCRP Report 38, 1971.
[10] A. Carpinteri, Cusp catastrophe interpretation of fracture instability, *Journal of the Mechanics and Physics of Solids* **37** (1989), 567.
[11] A. Carpinteri, A catastrophe theory approach to fracture mechanics, *International Journal of Fracture* **44** (1990), 57.
[12] G. Vola and M. Marchi, Quantitative phase analysis (QPA) of the Luserna Stone, *Period. Mineral.* **79**(2) (2009), 45–60.
[13] R. Sandrone, P. Cadoppi, R. Sacchi and P. Vialon, The Dora–Maira massif, in: *Pre-Mesozoic Geology in the Alps*, J.F. Von Raumer and F. Neubauer, eds, Springer, Berlin, 1993, p. 317.
[14] R. Compagnoni, G.M. Crisci and R. Sandrone, Caratterizzazione chimica e petrografica degli "gneiss di Luserna" (Massiccio cristallino Dora–Maira, Alpi Occidentali), *Rend. Soc. It. Min. Petr.* **38** (1982, 1983), 498.
[15] R. Sandrone, La Pietra di Luserna nella letteratura tecnico-scientifica, in: *Seminario Internazionale, Le Pietre Ornamentali della Montagna Europea*, 10–12 June, Luserna San Giovanni, Torre Pellice, 2001, p. 333.
[16] M. Kuzhevskij, O.Yu. Nechaev, E.A. Sigaeva and V.A. Zakharov, Neutron flux variations near the Earth's crust, A possible tectonic activity detection, *Natural Hazards and Earth System Sciences* **3** (2003), 637.
[17] M. Kuzhevskij, O.Yu. Nechaev and E.A. Sigaeva, Distribution of neutrons near the Earth's surface, *Natural Hazards and Earth System Sciences* **3** (2003), 255.
[18] N.N. Volodichev, B.M. Kuzhevskij, O.Yu. Nechaev, M.I. Panasyuk, A.N. Podorolsky and P.I. Shavrin, Sun–Moon–Earth connections: the neutron intensity splashes and seismic activity, *Astronomicheskii Vestnik* **34**(2) (2000), 188.
[19] G. Favero and P. Jobstraibizer, The distribution of aluminum in the Earth: from cosmogenesis to Sial evolution, *Coordination Chemistry Reviews* **149** (1996), 367.
[20] S.R. Taylor and S.M. McLennan, The geochemical evolution of the continental crust, *Reviews of Geophysics* **33**(2) (1995), 241.
[21] S.R. Taylor and S.M. McLennan, *Planetary Crusts: Their Composition, Origin and Evolution*, Cambridge Univ. Press, Cambridge, 2009.
[22] A.D. Anbar, Elements and evolution, *Science* **322** (2008), 1481.
[23] J.I.E. Lunine, *Earth: Evolution of a Habitable World*, Cambridge Univ. Press, Cambridge, 1998.
[24] R.M. Hazen et al., Mineral evolution, *American Mineralogist* **93** (2008), 1693.
[25] K.C. Condie, *Plate Tectonics and Crustal Evolution*, Pergamon Press, Elmsford, New York, 1976.
[26] I. Roy, B.C. Sarkar and A. Chattopadhyay, MINFO – a prototype mineral information database for iron ore resources of India, *Computers and Geosciences* **27** (2001), 357.
[27] World Iron Ore Producers, available at: http://www.mapsofworld.com/minerals/world-iron-ore-producers.html; last accessed October 2009.
[28] World Mineral Resources Map, available at: http://www.mapsofworld.com/world-mineral-map.htm; last accessed October 2009.
[29] Key Iron Deposits of the World, available at: http://www.portergeo.com.au/tours/iron2002/-iron2002depm2b.asp; last accessed October 2009.
[30] K.O. Konhauser et al., Oceanic nickel depletion and a methanogen famine before the Great Oxidation Event, *Nature* **458** (2009), 750.
[31] M.A. Saito, Less nickel for more oxygen, *Nature* **458** (2009), 714.
[32] R.L. Rudnick and D.M. Fountain, Nature and composition of the continental crust: a lower crustal perspective, *Reviews of Geophysics* **33**(3) (1995), 267.
[33] F. Egami, Minor elements and evolution, *Journal of Molecular Evolution* **4**(2) (1975), 113.
[34] National Academy of Sciences, Nickel Committee on Medical and Biological Effects of Environmental Pollutants, Nickel, National Academy of Sciences, Washington, DC, 1975.
[35] C. Doglioni, Interno della Terra, Treccani, in: *Enciclopedia Scienza e Tecnica*, 2007, pp. 595–605.
[36] B. Foing, Earth's childhood attic, *Astrobiological Magazine: Retrospection*, February 23, 2005.